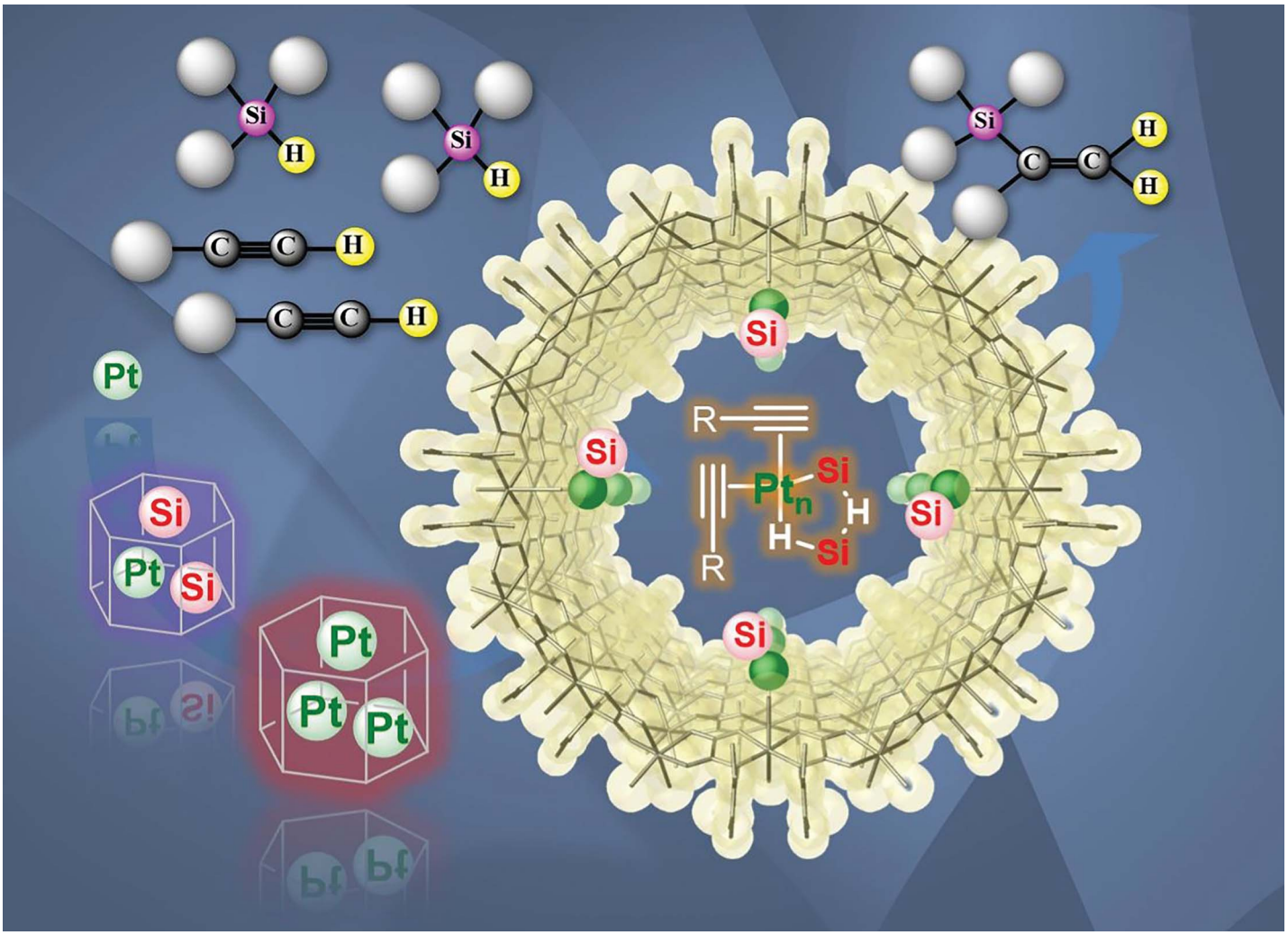

Showcasing research from Professor Leyva-Pérez's laboratory, Instituto de Tecnología Química. Universitat Politècnica de València–Consejo Superior de Investigaciones Científicas., Valencia, Spain.

Cyclic metal(oid) clusters control platinum-catalysed hydrosilylation reactions: from soluble to zeolite and MOF catalysts

The Pt–catalysed hydrosilylation reaction is a fundamental transformation in industrial and academic chemistry, however, the exact nature of the Pt active species and its mechanism of action is not well understood yet. Here, we show that the hydroaddition of alkynes proceeds through Pt–Si–H clusters of 3–5 atoms (metal(oid) association) in part–per–million amounts (ppm). This metal(oid) association relaxes hydrosilylation intermediates versus the accepted highly-strained Chalk-Harrod mechanism and enables solid catalyst design, which paves the way for more environmentally–benign industrial applications.

As featured in:

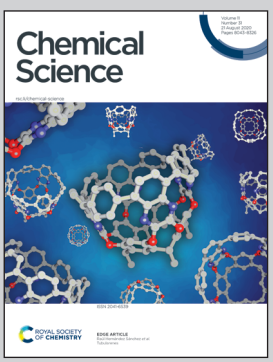

See M. Rivero-Crespo, J. P. Cerón-Carrasco, A. Leyva-Pérez *et al.*, *Chem. Sci.*, 2020, **11**, 8113.

ROYAL SOCIETY OF CHEMISTRY

rsc.li/chemical-science

Registered charity number: 207890

Chemical Science

ROYAL SOCIETY OF CHEMISTRY

EDGE ARTICLE

View Article Online
View Journal | View Issue

Cite this: *Chem. Sci.*, 2020, **11**, 8113

All publication charges for this article have been paid for by the Royal Society of Chemistry

Cyclic metal(oid) clusters control platinum-catalysed hydrosilylation reactions: from soluble to zeolite and MOF catalysts†

Miguel Rivero-Crespo,‡*[a] Judit Oliver-Meseguer,[a] Klaudia Kapłońska,[b] Piotr Kuśtrowski,[b] Emilio Pardo,[c] José Pedro Cerón-Carrasco*[d] and Antonio Leyva-Pérez*[a]

Received 28th April 2020
Accepted 5th July 2020

DOI: 10.1039/d0sc02391d

rsc.li/chemical-science

The Pt-catalysed addition of silanes to functional groups such as alkenes, alkynes, carbonyls and alcohols, *i.e.* the hydrosilylation reaction, is a fundamental transformation in industrial and academic chemistry, often claimed as the most important application of Pt catalysts in solution. However, the exact nature of the Pt active species and its mechanism of action is not well understood yet, particularly regarding regioselectivity. Here, experimental and computational studies together with an *ad hoc* graphical method show that the hydroaddition of alkynes proceeds through Pt–Si–H clusters of 3–5 atoms (metal(oid) association) in parts per million amounts (ppm), which decrease the energy of the transition state and direct the regioselectivity of the reaction. Based on these findings, new extremely-active (ppm) microporous solid catalysts for the hydrosilylation of alkynes, alkenes and alcohols have been developed, paving the way for more environmentally-benign industrial applications.

1 Introduction

The Pt-catalysed hydrosilylation of alkenes, alkynes, ketones and alcohols, among others, is the method of choice to obtain industrially-useful organosilanes, and unlike hydroborations or hydrostannylations, it only proceeds in the presence of a catalyst.[1,2] After 50 years of intensive research, Pt-based catalysts are still the catalysts of choice in both academia and industry due to their inherent and extremely high catalytic activity for this particular reaction, working in parts per million amounts (ppm), at room temperature and with good selectivity in some cases. The fact that the soluble Pt catalyst is not removed after the reaction and that the produced organosilanes are present in industrial silicones in multi-tonnes per year has led to a worldwide spread of the inherently toxic metal.[3a] Thus, the search for more benign hydrosilylation catalysts, with similar catalytic activity to soluble Pt but which do not remain in the final product, is not only a practical and economical but also a toxicological and environmental concern.[3]

Heterogeneous catalysis is considered a suitable solution when soluble catalysts are toxic and not recyclable, and the more direct and simple approach to heterogenise a soluble catalyst is by supporting it on a simple solid.[4] However, examples of truly heterogeneous Pt-supported solid catalysts for hydrosilylation reactions, which mimic the extremely high catalytic activity of Pt in solution, are difficult to find in the literature.[5] The main reason for this shortage of reported examples is that the exact nature of the catalytically active Pt species formed in solution during reactions, as well as the structure of key intermediates during the different hydrosilylation reactions, remains mainly unknown, beyond the postulated Chalk–Harrod intermediate shown in Fig. 1.[6] The extremely low amount of Pt required to catalyse the hydrosilylation of alkenes and alkynes in solution is well below the detection limits for many experimental techniques, which has precluded conclusive studies on Pt active species. If these catalytically active Pt reaction intermediates are properly detected, the design of new solid catalysts would be easier and more efficient.

Here, we show experimental and computational studies, together with the development of an *ad hoc* graphical method, which support the association of silane molecules with Pt atoms in solution, prior to or during the rate determining step (rds) of

[a]*Instituto de Tecnología Química, Universitat Politècnica de València–Consejo Superior de Investigaciones Científicas, Avda. de los Naranjos s/n, 46022, Valencia, Spain. E-mail: miguel_angel.rivero_crespo@org.chem.ethz.ch; anleyva@itq.upv.es; Fax: +34963877809; Tel: +34963877800*

[b]*Faculty of Chemistry, Jagiellonian University, Gronostajowa 2, 30-387 Krakow, Poland*

[c]*Instituto de Ciencia Molecular (ICMol), Universidad de Valencia, 46980 Paterna, Valencia, Spain*

[d]*Reconocimiento y Encapsulación Molecular (REM), Universidad Católica de Murcia (UCAM), Spain. E-mail: jpceron@ucam.edu*

† Electronic supplementary information (ESI) available: General procedures, additional tables, figures and movies, and compound characterization. See DOI: 10.1039/d0sc02391d

‡ Current address: Department of Chemistry and Applied Biosciences, Swiss Federal Institute of Technology (ETH) Zürich, Vladimir-Prelog-Weg 1-5/10, 8093 Zürich, Switzerland.

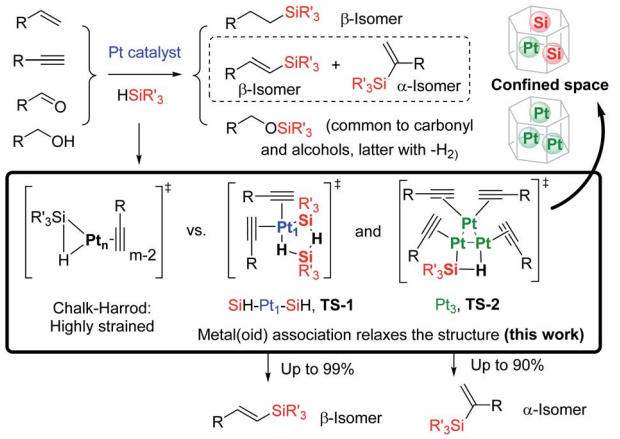

Fig. 1 Pt-catalysed hydrosilylation of alkenes, alkynes, ketones and alcohols. The inset shows the postulated Chalk–Harrod intermediate and the regioselective **TS-1** and **TS-2** cyclic metal(oid) intermediates proposed in this work, with the extension to confined spaces in solid catalysts.

the reaction, to generate 3–5 atom cyclic metal(oid) clusters that facilitate the reaction by providing an alternative low-energy pathway to the classical Chalk–Harrod mechanism. It is also shown here how these cyclic metal(oid) clusters control the electronics and sterics during the alkyne hydrosilylation and govern the final chemo-, regio- and stereoselectivity of the reaction, and with this information in hand, new and extremely active soluble and solid-supported Pt catalysts can be designed not only for the hydrosilylation of alkynes but also for the hydrosilylation of alkenes and alcohols.

2 Results and discussion

2.1. Homogeneous catalysis

2.1.1 Kinetic experiments and a graphical method unveil metal(oid) cluster formation during the hydrosilylation of alkynes. Ligand-free Pt_1 and Pt_3 were synthesised under typical reaction conditions for the hydrosilylation of alkynes, and this reaction was selected since, in contrast to alkenes, alkyne hydrosilylation involves both regio- and stereoselectivity features.[7,8] For the study, the classical Karstedt hydrosilylation catalyst [Pt^0-1,3-divinyl-1,1,3,3-tetramethyldisiloxane] was treated with 10 mol% of 2,2,6,6-tetramethylpiperidine 1-oxyl (TEMPO) or not, to give ligand-free Pt_1 or Pt_3, respectively, in >90% yield according to combined mass spectroscopy and ultraviolet-visible absorption and emission spectroscopy.[9] This methodology, validated by comparative studies with single-atom supported Pt_1 solids[5b] and preformed Pt_3 Chini clusters[10,11] ($[Pt_3(CO)_6]_5^{2-}$) in solution, at different temperatures, enables the study of the catalytic action of both Pt species during the hydrosilylation reaction without the interference of any ligand beyond the very same reactants,[12] thus avoiding any modification of the intrinsic catalytic activity associated with the bare Pt atoms.[13] As expected, bigger Pt clusters and nanoparticles are not the catalytically active species during the hydrosilylation reaction, since a very clear induction time can be observed when using Pt NPs supported on carbon as a catalyst.[9,14]

The results in Fig. 2 [see also Fig. S1–S3 in the ESI†] show the rate equations for the hydrosilylation of phenylacetylene **1** with triethylsilane **2** catalysed by either Pt_1 or Pt_3, obtained from the initial kinetic points, which are $r_0 = k_{exp}[Pt_1][\mathbf{1}]^{-1}[\mathbf{2}]^2$ and $r_0 = k_{exp}[Pt_3][\mathbf{1}]^{-1}[\mathbf{2}]$, respectively. In other words, the hydrosilylation reaction rate is, in both cases, linearly proportional to the amount of Pt and inversely proportional to the amount of alkyne but, unexpectedly, it is quadratically proportional to the amount of silane for Pt_1 but not for Pt_3. For the latter, saturation kinetics is observed at high silane concentrations ([**2**] > 0.50 M). It is noteworthy that the main product for Pt_1 is the typical β-(*E*) alkenylsilane,[15] with >95% selectivity, while for Pt_3 is the less common α-alkenylsilane,[9,16] with >90% selectivity. However, here the formation of both products is equally considered to assess the catalytic activity of the different Pt catalysts.

A Hammett plot for different *para*-substituted dimethylphenylsilanes prepared by a reported method[17] gives a similar negative slope for both catalysts ($\rho_{Pt_1} = -0.50$, $\rho_{Pt_3} = -0.60$, Fig. S4†), and the kinetic isotope effect (KIE) values for the hydrosilylation of **1** with H(D)$SiEt_3$ are 2.0 and 1.7 ± 0.2 for Pt_1 and Pt_3 respectively (see further below for a more precise value through the graphical method), which confirm that a positive charge is being built and that the Si–H(D) bond is breaking before or during the rate determining step of the hydrosilylation reaction, for both Pt_1 and Pt_3 catalysts respectively. However, this catalytic similarity between Pt_1 and Pt_3 is clearly broken when considering the enthalpy and entropy values in the transition state ($\Delta H^{\ddagger}$ and $\Delta S^{\ddagger}$). Table 1 shows the $\Delta H^{\ddagger}$ and $\Delta S^{\ddagger}$ values for the hydrosilylation reaction of **1** with **2**, calculated experimentally with the Eyring–Polanyi equation, and the results show that the Pt_1 catalyst significantly decreases both the enthalpy and entropy values (~50 kJ mol^{-1} and −190 J K^{-1} mol^{-1}, respectively, entry 1) relative to Pt_3 (~110 kJ mol^{-1} and −25 J K^{-1} mol^{-1}, entry 2), which raises the apparent contradiction that the transition state is more associated for Pt_1 than for Pt_3. To assess the influence of the alkyne and the silane on the $\Delta H^{\ddagger}$ and $\Delta S^{\ddagger}$ values, the study was expanded to 1-octyne **3**

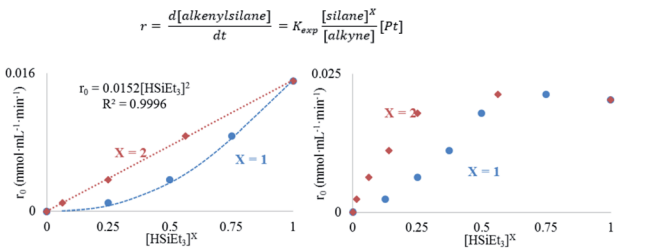

Fig. 2 Top: Experimental kinetic equation for the Pt-catalysed hydrosilylation reaction. It should be noted that [silane] is raised to the power of *X*. Bottom: Reaction rate for the hydrosilylation of phenylacetylene **1** *vs.* [$HSiEt_3$] and $[HSiEt_3]^X$ ($X = 1$ or 2) for either Pt_1 (left) and Pt_3 (right) at increasing amounts of triethylsilane **2** maintaining [**1**] constant, with the Kardstedt catalyst (2.5×10^{-5} M) and TEMPO (only in left graphic, 0.05 M); toluene (1 ml), and 110 °C reaction temperature.

Table 1 Transition state enthalpy and entropy values for the hydrosilylation of phenylacetylene **1** or 1-octyne **3** (0.5 M) with triethylsilane **2** (0.6 M) or 1,1,3,3-tetramethyldisiloxane **4** (TMDS, 0.125 M) catalysed by Pt_1 and Pt_3 (2.5×10^{-5} M). Reactions carried out at temperatures of 80, 95, 110 and 125 °C. In brackets values obtained by the graphical method

Entry	Alkyne/silane	Pt	$\Delta H^{\ddagger}$ (kJ mol^{-1})	$\Delta S^{\ddagger}$ (J K^{-1} mol^{-1})
1	**1**/**2**	Pt_1	53 ± 4 (52 ± 2)	−175 ± 10 (−156 ± 6)
2		Pt_3	114 ± 6 (109 ± 2)	−2 ± 16 (5 ± 6)
3	**3**/**2**	Pt_1	52 ± 3 (54 ± 3)	−171 ± 8 (−168 ± 15)
4		Pt_3	103 ± 12 (123 ± 4)	22 ± 33 (40 ± 17)
5	**1**/**4**	Pt_1	24 ± 3 (38 ± 2)	−252 ± 9 (−210 ± 20)
6		Pt_3	28 ± 3 (41 ± 2)	−242 ± 6 (−188 ± 5)

and 1,1,3,3-tetramethyldisiloxane (TMDS) **4**, and the results (entries 3–6) show that a different alkyne does not modify the energetics of the transition state while a different silane indeed does. These results fit with the different reaction order found with respect to the Pt atomicity for the silane but not for the alkyne and suggest that not only the nature but also the number of silane molecules is key in the transition state of the hydrosilylation reaction, at least with Pt_1.

In order to confirm these energetic differences, a more accurate graphical method was developed, since the initial rate approximation encounters some limitations in reactions with induction times, catalyst deactivation, late steady state attainment and very fast rates,[18] which can be the case here. In this context, Reaction Progress Kinetic Analysis (RPKA)[19] and Variable Time Normalization Analysis (VTNA)[20] have emerged in recent years as powerful tools to measure reaction orders from catalysed reactions with high precision in few experiments.[21] However, both RPKA and VTNA do not cover other kinetic and thermodynamic parameters such as the transition state enthalpy and entropy, linear free energy relationships (LFER) and KIE (Fig. S5†).[22] Despite temperature scanning methodologies having been recently developed to calculate energetic activation parameters,[22d] this methodology is much more complex in terms of instrumentation and data treatment. For all these reasons, and inspired by the simple graphical methodologies mentioned above, a graphical method to calculate the $\Delta H^{\ddagger}$, $\Delta S^{\ddagger}$, Hammett parameter (ρ) and KIE values, using the tools available in our laboratory, was developed here. This new methodology does not only allow the calculation of the energetic values with high precision in few experiments, but also proposes a way to calculate the errors associated with the measurements (see the ESI† for discussion).

Fig. 3 illustrates the basis of our approach for a simulated bimolecular reaction A + B → P, *i.e.* the hydrosilylation reaction, with the calculation of the transition state enthalpy and entropy values ($\Delta H^{\ddagger}$ and $\Delta S^{\ddagger}$, see the ESI† for the mathematical model development). The final methodology is very simple and involves representing the product concentration *vs.* the normalized time-scale *f* or $g(t, T, \Delta H^{\ddagger}$ or $\Delta S^{\ddagger})$. In this way, the transition state enthalpy $\Delta H^{\ddagger}$ or entropy value $\Delta S^{\ddagger}$ is easily obtained by iterations with any available user graphic software (Excel®, Origin®, …) until all kinetic profiles overlay at different temperatures, which can be done either by just visually, adjusting to a polynomic equation until obtaining the best fit in terms of R^2 or by minimizing the Euclidean distance between the data points. The latter approach was used in this work (see the ESI†). This methodology gives the activation parameters directly from raw concentration data, avoiding the propagation of errors associated with the initial rates, which can be as high as ±8% at $R^2 = 0.997$ for the classical method (Fig. S6 and Tables S1–S5†), but only up to ±4% at nearly perfect fittings ($R^2 > 0.999$) for the new graphical method. Noteworthily, the graphical method overrides the experimental distortions arising from induction times, since these induction times are included in the whole kinetic profile, which was validated for a simulated (Fig. S7, S8, Tables S6 and S7†) and a reported related reaction[23] (Fig. S9†).

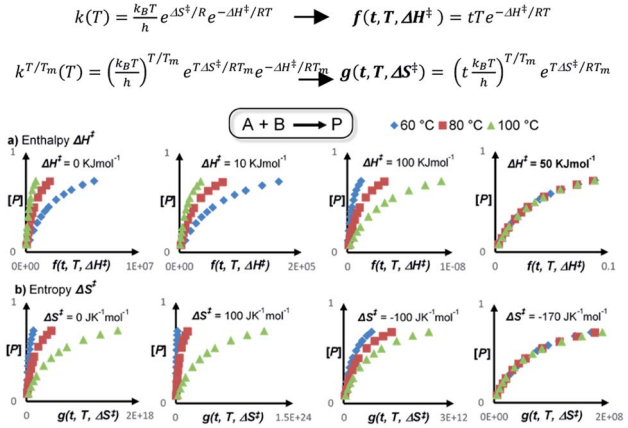

Fig. 3 Top: Equations employed in the graphical method to obtain the enthalpy and entropy transition state values $\Delta H^{\ddagger}$ and $\Delta S^{\ddagger}$. Bottom: Examples of transition state enthalpy (a) and entropy (b) calculations using the time-normalized scales *f* and *g* respectively for a bimolecular reaction carried out at three different temperatures: 60, 80 and 100 °C.

The results of $\Delta H^{\ddagger}$ and $\Delta S^{\ddagger}$ obtained by the graphical method are shown in Table 1 (see also Fig. S10–S15†) and reinforce the conclusions obtained with the traditional kinetic values, *i.e.* the transition stateis less energetic (lower $\Delta H^{\ddagger}$) and more associated (lower $\Delta S^{\ddagger}$) for Pt_1 than for Pt_3. Fig. 4 shows that the graphical method can also be applied to find the Hammett parameter (ρ, Fig. S16 and Tables S8–S10†) and KIE values (see the ESI† for discussion), which gives $\rho = 0.50$ for the Pt_1 catalyst and KIE = 1.91(5) for the Pt_3 catalyst, exactly the same value as that for Pt_1 but with much more precision (see above and Table S11†).

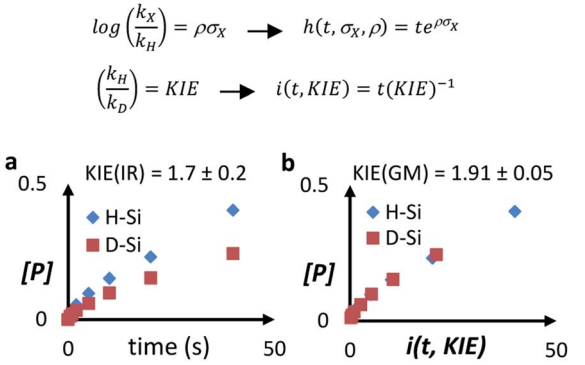

Fig. 4 Top: Equations employed in the graphical method to obtain the Hammett value (ρ) and the KIE. Bottom: Kinetic profiles and KIE values calculated by the (a) initial rates (IR) method and (b) graphical method (GM), for the Pt_3 catalyst.

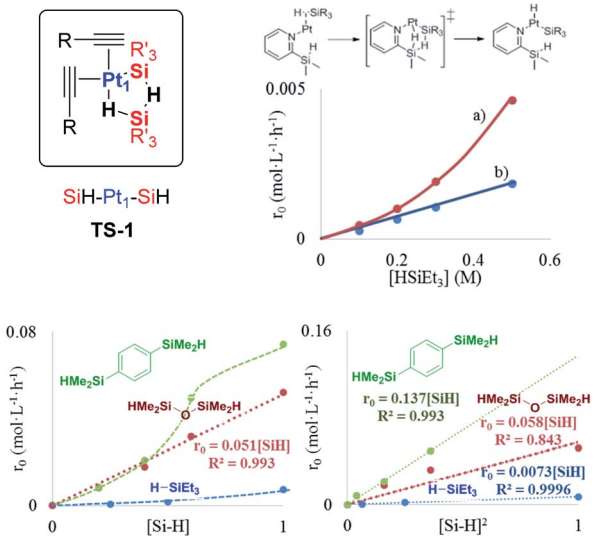

Fig. 5 Top left: Proposed transition state **TS-1** during the hydrosilylation of alkynes with the Pt_1 catalyst. Top right: Reaction rate for the hydrosilylation of phenylacetylene **1** (0.5 M) with triethylsilane **2** using *in situ* generated Pt_1 from Kardstedt's catalyst (2.5×10^{-5} M) without (a) or with silanepyridine **6** (b). Bottom: Reaction rate for the hydrosilylation of phenylacetylene **1** (1 M in toluene) with *in situ* generated Pt_1 from Kardstedt's catalyst (2.5×10^{-5} M) at 110 °C, with respect to the (a) silane concentration and (b) squared silane concentration, with silanes **2**, **4** and **5**.

These results confirm the energetic and isotopic kinetic data obtained for the hydrosilylation of alkynes with Pt_1 and Pt_3, and support the hypothesis of metal(oid) Pt–silane cluster formation during the transition state of the reaction.

2.1.2 Reactivity experiments support a cyclic metal(oid) cluster. The observed change in the silane reaction order from +1 to +2 at low [silane] for Pt_1, indicates that two silane molecules are involved in the mechanism either in a separate, sequential or cooperative manner, which clearly deviates from the Chalk–Harrod mechanism, modified or not.[24] To shed light on this, the hydrosilylation of **3** with equimolecular amounts of $HSiEt_3$ and $DSiPr_3$ was carried out, and the formation of a mixture of deuterated and non-deuterated scrambled hydrosilylation products, together with scrambled reactants ($DSiEt_3$ and $HSiPr_3$), was observed by gas chromatography coupled to mass spectrometry (GC-MS) in the first few minutes of the reaction, which discards that two separate Si–H units operate during the reaction. Two consecutive and reversible oxidative additions of the silane to the Pt(0) atom are very unlikely since it would lead to a highly energetic Pt(IV) intermediate. Considering that the oxidative addition of non-polar bonds such as Si–H is expected to occur *via* a concerted and not S_N2 mechanism,[25a] a more reasonable interpretation is the cooperative formation of a transition state with two silane molecules bound to the Pt_1 atom, which is represented in Fig. 5 (see also Fig. 1). In this cyclic structure, named **TS-1**, two silane molecules would form a five-membered ring with the Pt_1 atom to enable a cooperative oxidative addition through a less strained transition state, which resembles reported intermediates for the Pd-catalysed Wacker oxidation[25b] and Au_2-catalysed oxidative heteroarylations,[25c] the former with three water molecules forming a chain coordinated to Pd in the key oxypalladation step. **TS-1** explains why TMDS **4** decreases the activation energy (see Table 1), since disilane **4** acts as a bidentate molecule for easily generating the cyclic intermediate.[26] If this is the case, **4** should have a first order dependence in the rate equation, which is indeed observed in Fig. 5; the kinetics of the hydrosilylation of **1** with disilane **4** bearing two flexible Si–H moieties close to each other, shows a much better first order [silane] dependence, and **1** reacts much faster than monosilane **2**. Conversely, a rigid disilane molecule such as 1,4-bis(dimethylsilyl)benzene **5**, bearing two Si–H moieties far away from each other and incapable of forming a 5-membered ring, still shows a quadratic $[silane]^2$ dependence, as it occurs with triethylsilane **2**. Moreover, Fig. 5 also shows that 2-(dimethylsilyl)pyridine **6** acts as a functional ligand for Pt_1, placing a Si–H bond at an appropriate distance to form a double five and six-membered ring with the incoming silane and showing a linear [silane] dependent rate, faster at low silane concentrations than with naked Pt_1 (Fig. S17†). It can noted that hydrosilylation between the alkyne reagent and the ligand does not occur, and thus the ligand remains unaltered during the reaction, and that the highly coordinating nature of the pyridine moiety gives a less active homogeneous catalyst than Pt_1 at higher concentrations. These results, together, strongly support that the negative transition state entropy measured for Pt_1 corresponds to a highly associative, cyclic metal(oid) transition state such as **TS-1**, which directs the anti-Markovnikov hydrosilylation of alkynes and gives the β-(*E*) alkenylsilane products.

The occupancy of the free coordinating sites in **TS-1** by alkynes is supported by the negative dependence of the hydrosilylation rate on the alkyne concentration, for both Pt_1 and Pt_3 catalysts, which indicates that the saturation of the coordinative sites of Pt with alkyne molecules occurs at the very beginning of the catalytic cycle, in accordance with the alkynophilic nature of the metal. This hypothesis is supported by the enhanced reaction rate found for electron-rich alkynes (worse π-acceptors), following the order: electron-deficient phenylacetylenes < electron-rich phenylacetylenes < alkyl alkynes, assessed by the

negative slope in the Hammett plot (Fig. S18†), and the decrease in the reaction rate when phenylacetylene **1** is added during the hydrosilylation of 1-octyne **3**, but not the reverse, in accordance with the stronger π-accepting ability of **1** (Fig. S19†), and the lack of the kinetic isotope effect (KIE) found for deuterated phenylacetylene (1.1 ± 0.1 for both Pt_1 and Pt_3), which indicates that σ-Pt alkynylide species do not participate in the reaction. Thus, the incoming silane must displace coordinating alkyne molecules in the inner sphere of Pt through σ-interactions,[27] to give the key cyclic metalloid cluster.

A four-membered metal(oid) cyclic transition state may also be involved for Pt_3 clusters, in this case with just one silane molecule, shown in Fig. 6 as **TS-2** (see also Fig. 1). The linearity of the rate equation with [**2**] (see above) supports this intermediate. Furthermore, taking advantage of the different regioselectivity found for Pt_3 and the fact that the regioselectivity comes from the electronic effect produced by alkyne polarization, the reactivity of different internal alkynes where the two carbon atoms are electronically similar, was tested. Fig. 6 also shows that no α/β differentiation occurs between Pt_1 and Pt_3 catalysts while, in contrast, an extremely polarized internal alkyne such as trimethylsilylphenylacetylene **7**, where the charge difference between the two carbon atoms is comparable to a terminal alkyne (Table S12†), produces a change in the α/β isomer ratio from 0.37 (Pt_1) to 0.60 (Pt_3). These results support that the electronics of the alkyne is determinant for the regioselectivity during the Pt_3-catalysed hydrosilylation reaction, but not with the Pt_1 catalyst.[28] Regarding sterics, electronically similar *ortho*- and *para*-substituted phenylacetylenes show that the former react less with Pt_1 clusters than with Pt_3 (Fig. 6, S20 and S21†), and these results make sense considering that the cyclic metal(oid) transition state around Pt_1 is more congested than around Pt_3, thus enhancing steric effects during the reaction (Fig. S21†).[29] The so-called *ortho* effect, initially described for the hydrostannylation of alkynes[30] and associated with higher differences in ^{13}C NMR for internal and external carbon atoms, cannot be invoked here since it is caused not only by electronic but also by steric effects.[31] Two-dimensional nuclear magnetic resonance nuclear Overhauser effect spectroscopy (NOESY) of the α-vinylsilane product, deuterated or not, shows that both the anti- and Markovnikov hydrosilylation reactions with Pt_1 and Pt_3 proceed completely in a *syn*-fashion (Fig. S22–S24†), which is in accordance with the observed products and previous studies on silylplatination and reductive elimination steps.[32]

2.1.3 Computational studies support the energetic feasibility of the cyclic metal(oid) cluster TS-1. Aiming at further assessing the energetic preference for the different transition states during the hydrosilylation reaction, density functional theory (DFT) calculations have been systematically conducted for the oxidative addition and hydroplatination steps, for both the proposed metal(oid) cluster **TS-1** and Chalk–Harrod intermediate (**TS-3**). For the records, the locations of both hydrogen and silicon atoms have been monitored during the reaction with propyne, which is used here as a minimal model system of an alkyne moiety. Fig. 7 summarizes the predicted energetic changes for both α and β products, and the nature of the transition states is confirmed by analysing the vibrational normal modes associated with the reaction coordinate (Movies S1–S4 in the ESI†).

According to the calculations, the proposed **TS-1** metal(oid) cluster decreases the barrier for the hydride addition (intermediates [A]) by *ca.* 10 kcal mol^{-1} (black and blue lines) with

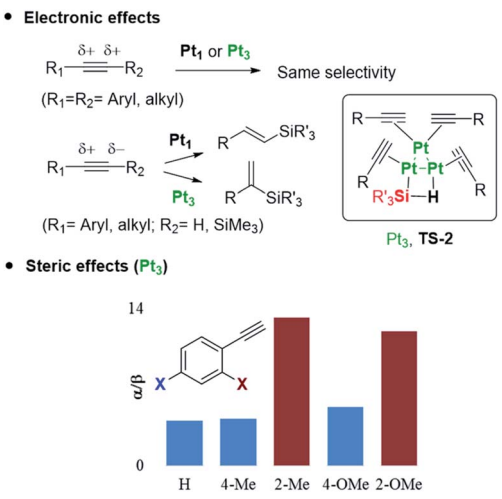

Fig. 6 Proposed transition state **TS-2** during the hydrosilylation of alkynes with the Pt_3 catalyst, and electronic and steric factors of the alkyne affecting reaction regioselectivity for Pt_3.

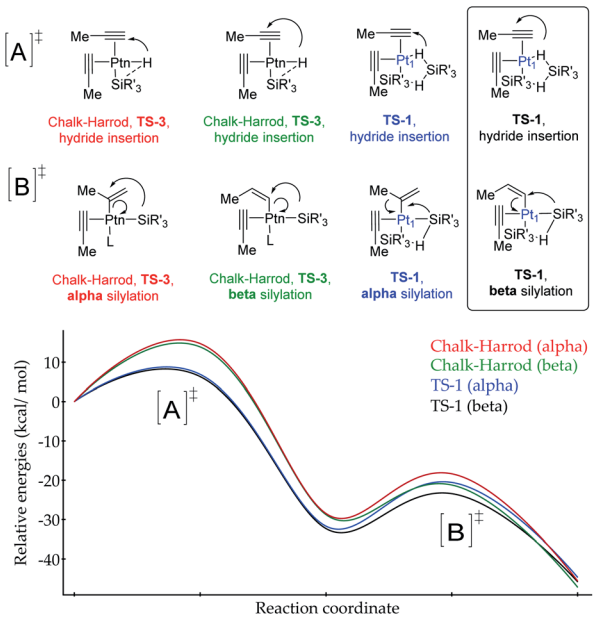

Fig. 7 Computed energy profile for the Pt-catalysed Markovnikov (alpha product) and classical anti-Markovnikov (beta product) hydrosilylation of propyne. [A] refers to the hydride insertion step and [B] to the silylation step (L refers to a propyne or solvent molecule, not involved in the calculations). The red and green lines illustrate the predicted reaction by using the standard Chalk–Harrod mechanism (**TS-3**), while the blue and black curves stand for the reaction through two silane molecules bound to a single Pt_1 atom (**TS-1**). In all cases, both α and β products are simulated.

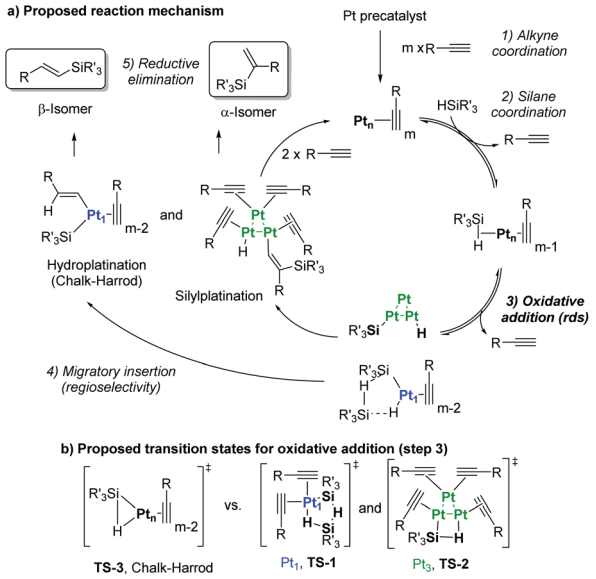

Fig. 8 (a) Chalk–Harrod mechanism ($n = 1$) and the alternative mechanism found in this work ($n = 1$ and 3). (b) Transition states for the oxidative addition proposed in this study.

respect to the standard Chalk–Harrod intermediate **TS-3** (red and green lines), regardless of the regiochemistry of the product. This stabilization comes from the significantly less constrained environment around the Pt atom when two silane molecules bind and cooperate, compared to the canonical Chalk–Harrod configuration. Furthermore, the smallest energy barrier for the final silylation step (intermediates [B]) corresponds to the formation of the β-isomer through the **TS-1** intermediate (black line), and thus the DFT calculations predict the right product after a silane self-assisted hydroplatination process. All these accumulated theoretical outcomes back up the hypothesis of cyclic metal(oid) cluster formation.

2.1.4 Proposed reaction mechanism and complete kinetic equations for the Pt-catalysed hydrosilylation of alkynes. Fig. 8 shows a plausible reaction mechanism, on the basis of the above experiments and compared with the classical Chalk–Harrod mechanism. The first steps are similar to those of the accepted Chalk–Harrod mechanism,[1,7,24] *i.e.* (1) alkyne coordination to Pt, (2) silane coordination and (3) oxidative addition of the silane. However, at this point, the metal(oid) cluster association occurs, and the reaction follows a different reaction pathway depending on the type of Pt–silane cluster formed. If two silane molecules bind to a single Pt_1 atom (**TS-1**), migratory insertion through a silane self-assisted hydroplatination process is favored and an anti-Markovnikov product is formed after reductive elimination. In contrast, if one silane molecule binds the Pt_3 cluster (**TS-2**), the Markovnikov regioselectivity is preferred by the cooperative dissociation of one silane molecule on the Pt_3 cluster, to give a regioselective silylplatination of the polarized terminal alkyne. Of course, a direct visualization of **TS-1** and **TS-2** by experimental techniques such as NMR or X-ray spectroscopy is not possible, and although this visualization would be desirable for **III-A** and **III-B** to confirm the proposed mechanism, the extraordinary level of dilution of the ligand-free Pt catalyst during the hydrosilylation reaction (10^{-5} M) must be taken into account, which discards any of these techniques for reliable data. In any case, the here proposed cyclic metal(oid) clusters are more elaborated, precise and energetically-favored intermediate species for the hydrosilylation alkynes compared to the postulated, canonical and highly strained 3-membered-ring transition state in the Chalk–Harrod mechanism. It is noteworthy that earlier ultrasmall Rh clusters were reported as an active catalyst for the hydrosilylation of alkynes,[33] and other noble metal clusters (including Pt) can be easily formed under similar reaction conditions and catalyse related reactions such as the hydrogenation of alkenes,[34] carbene-mediated couplings[35] and carbon–carbon cross-coupling reactions.[14,36]

Taking into consideration the elementary steps of the mechanism proposed in Fig. 8, validated not only by experimental results but also by computational results and the graphical method, a theoretical kinetic equation for the Markovnikov hydrosilylation of alkynes catalysed by Pt_1 can be obtained, using the steady state approximation (Fig. S25† for mathematical development). With the appropriate simplifications, the resulting calculated equation resembles the experimentally obtained equation (*vide supra*), with the quadratic [silane]^2 dependence:

$$\text{Rate } Pt_1 = \frac{k_1k_2k_3}{(k_{-1}[A]+k_1[S])(k_{-2}[A]+k_3)+k_2\left(k_3k_5[A]^2+k_1[S]\right)[S]}[S]^2\left[Pt^0\right]$$

which can be approximated at low [silane]:

$$\text{Rate } Pt_1 = \frac{k_1k_2k_3}{(k_{-1}[A])(k_{-2}[A]+k_3)}[S]^2\left[Pt^0\right]$$

and the same applies for the Pt_3 catalyst (Fig. S26†), which gives the expected reaction orders after simplifications:

$$\text{Rate } Pt_3 = \frac{k_1k_2k_3}{k_2k_3+(k_{-2}+k_3)(k_{-1}[A]+k_1[S])}[S]\left[Pt^0\right]$$

Therefore, the mechanism in Fig. 8 is supported not only by kinetic, isotopic, thermodynamic and computational data, but also by the theoretical rate equations.

2.2. Heterogeneous catalysis

2.2.1 Hydrosilylation of alkynes. Solid catalysts are preferred in industry because they can be easily separated from the reaction media and recycled, or engineered in continuous processes. The cyclic metal(oid) transition states of low entropy **TS-1** and **TS-2**, with molecular sizes of around 1–2 nm, are formed under very diluted reaction conditions since the formation of >3 atom Pt aggregates is somehow hampered, and intramolecular reactions are favored *vs.* intermolecular ones. Thus, a solid catalyst with the ability to compartmentalize the active Pt species may mimic this catalytic behavior, and microporous solids with nanometric channels and cavities where Pt atoms can be accommodated, stabilized and electronically tuned, such as zeolites and metal–organic frameworks (MOFs), are thus suitable candidates to design Pt-

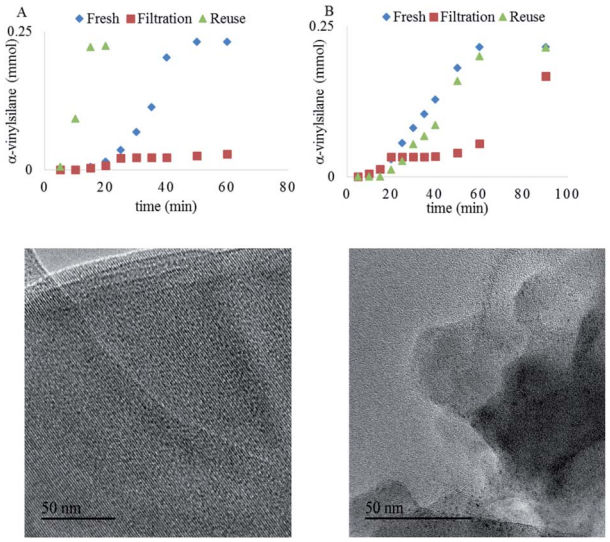

Fig. 9 Top: Hydrosilylation of 1-octyne **3** (0.5 M) with triethylsilane **2** (1.2 equivalents) in toluene (1 ml) at 110 °C using Pt_1/NaY (A) and Pt_3/NaY (B) as catalysts (2.5×10^{-4} M). Bottom: High resolution transmission electron microscopy (HR-TEM) images of the Pt_1/NaY catalyst (A) fresh and (B) reused 5 times.

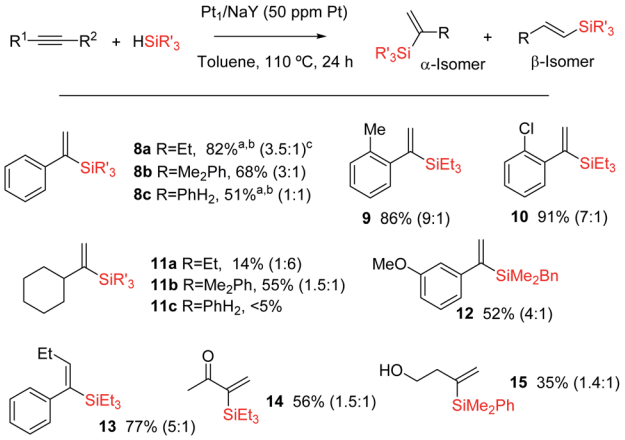

Fig. 10 Hydrosilylation of alkynes (0.5 M) with silanes (1.2 equivalents) in toluene (1 ml) at 110 °C using Pt_1/NaY (0.5 mg, 50 ppm in Pt) as a catalyst. [a] 61% at 25 °C reaction temperature with twenty times more catalyst. [b] GC yield of the α isomer after full conversion; isolated yields can be achieved with the oxidation method in 5–10% lower amounts. Not all products were isolated. [c] α/β ratio at the maximum conversion measured.

supported catalysts for the hydrosilylation of alkynes. The nanometric confined space of these microporous materials is a convenient place to maximize the cyclic metal(oid) formation, not only due to the size but also due to the intrinsic weak interactions of the metal and reactants with the framework walls, which assists in further reducing the entropy of the transition state.[37] Recent protocols describe the precise incorporation of isolated Pt_1 atoms and Pt clusters within the channels of zeolites and MOFs, and thus it is not necessary to develop new synthetic methodologies but just, perhaps, to apply and optimize known materials.[38] Thus, 1 wt% of Pt single atoms and Pt_3 clusters were incorporated into the typical NaY zeolite by reported methods (Pt_1/NaY[38a] and Pt_3/NaY[39] respectively), and the kinetic results for the hydrosilylation of 1-octyne **3** with triethylsilane **2** catalysed by these solid materials are shown in Fig. 9.

Both Pt_1/NaY and Pt_3/NaY, in ppm, give the α-vinylsilane product, but while Pt_1/NaY showed a long induction time (~25 minutes) and no leaching of Pt into solution, as assessed by the hot filtration test (Fig. 9A) and ICP analysis (<1% of supported Pt into solution), Pt_3/NaY showed, in contrast, a shorter induction and leaching of inactive Pt species into the solution (~10% measured by ICP), which evolve to active species after 50 minutes (Fig. 9B). In a similar way to Pt_3 clusters being formed *in situ* in solution from simple homogeneous precursors,[9,16] we reasoned here that Pt atoms inside Pt_1/NaY could also evolve to form Pt_3 clusters under reaction conditions, remaining within the zeolitic framework, while the pre-formed Pt_3 clusters inside the zeolite Pt_3/NaY are less stabilized by the framework and tend to leach out, which converts the Pt_3/NaY just to a simple reservoir of Pt.

Fig. 9A also shows that the Pt_1/NaY catalyst could be reused without any induction time (up to five times), without loss of activity and with just a small fraction of the confined Pt_3 aggregates being converted into nanoparticles (<2 nm),[40] according to high resolution transmission electron microscopy (HR-TEM) measurements (Fig. 9, bottom). These results strongly support that the active Pt_3 species are formed *in situ* and stabilized within the zeolite framework, ready to be further reused without leaching. In accordance with the leaching results, the preformed Pt_3/NaY sample loses activity and still shows some induction time (Fig. 9B).

Fig. 10 shows the results for the hydrosilylation reaction of different alkynes and silanes catalysed by Pt_1/NaY, and it can be seen that just 1 mg of the zeolite per mmol of alkyne (50 ppm of Pt) is enough to achieve full conversion and good selectivity towards the corresponding α-vinylsilanes, including aromatic (products **8a–c–10** and **12–13**) and alkyl alkynes (products **11a,b** and **14–15**), aromatic (products **8b,c**, **11b**, **12** and **15**) and alkyl silanes (products **8a–11a** and **14–14**), and also an internal alkyne (product **14**). Monosusbtituted phenylsilane $PhSiH_3$ reacts selectively once with an aromatic alkyne to give the corresponding silane **8c** in reasonable 51% yield (the rest is β isomer and not polyalkylated silanes), and it does not react with an alkyl alkyne (product **11c**). The silane $HSi(OEt)_3$ did not yield the desired product either, in any case, but rather decomposed. The reaction can also be run at room temperature, provided that more solid catalyst (20 mg per mmol of alkyne) is used, and this result indicates that the active and zeolite-stabilized Pt_3 species can be formed inside the zeolite without thermal requirements. To our knowledge, this is the first efficient and recyclable solid catalyst for the Markovnikov hydrosilylation of alkynes.[41] Previous tests[9] showed that Pt/C does not really work as a catalyst to obtain the alpha product but just generate species in solution with low alpha selectivity. Besides, not only the selectivity but also the activity is considerably higher in Pt/zeolites than in Pt/C. At this stage, and in order to

Table 2 Results for the hydrosilylation of styrene **16** (0.5 M) with dimethylphenylsilane **17** (1.2 equivalents) to give (2-phenylethyl) dimethylphenylsilane **18** with different soluble and solid Pt catalysts (100 ppm); acac = acetylacetonate, COD = cyclooctadiene. GC yields using *n*-dodecane as an external standard. Only the β isomer product was found

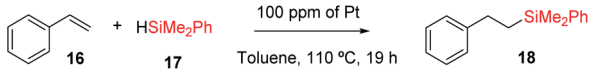

Entry	Pt catalyst	Yield (%)	TOF_0 (h^{-1})
1	Karstedt	86	455
2	$Pt(acac)_2$	75	393
3	$Pt(NH_3)_4Cl_2 \cdot xH_2O$	14	73
4	$Pt(COD)(Me)_2$	89	466
5	Pt/C	90	477
6	$PtCl_2/SiO_2$	6	31
7	Pt_1/NaY	96	514
8	**Pt_1/MOF**	**100**	**453**
9	**Pt_1/NaY (calc. at 200 °C)**	**100**	**526**

gain more information about the Pt species on the solid during the reaction, a ^{195}Pt solid NMR experiment was envisaged; however, the acquisition time to have a reliable result was estimated to be unacceptably long.

2.2.2 Hydrosilylation of alkenes. The catalyst of choice in the literature and in industry for the hydrosilylation of alkenes is the same as that for alkynes, *i.e.* Karstedt's catalyst.[42] Indeed, the Chalk–Harrod mechanism for alkynes has just been accommodated for alkenes according to previous studies,[7,24] thus, it may be expected that the solid Pt catalysts shown here could be applicable for the hydrosilylation of alkenes, particularly Pt_1/NaY.[5b,43] Table 2 shows the results for the hydrosilylation of styrene **16** with dimethylphenylsilane **17** with 100 ppm of different soluble and solid Pt catalysts, and it can be seen that not only Pt_1/NaY (entry 7) but also a recently reported Pt_1/MOF solid catalyst[38b] (entry 8) gives the best yields of terminal silane product **18** with initial turnover frequencies (TOF) comparable to those with Karstedt's catalyst (entry 1). It should be noted that a solid silica catalyst with supported $PtCl_2$, without removing the chloride anions, gives a marginal yield, while Pt/C gives good yields after long induction times, in accordance with the literature.[44]

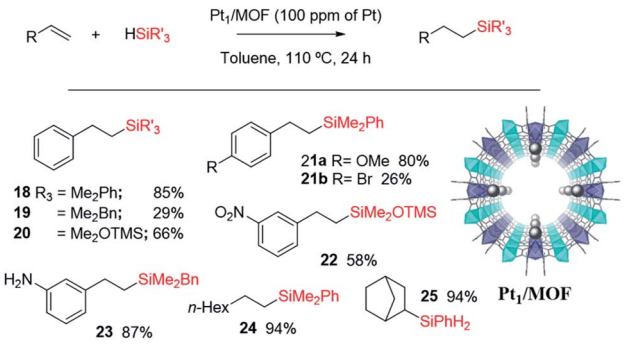

Fig. 11 Single crystal X-ray diffractogram of the Pt_1/MOF catalyst (the arrow marks the Pt atoms, grey balls) and scope for the hydrosilylation of terminal alkenes. NMR yields using dibromomethane as an internal standard. Only the β isomer product was found. Products were generally not isolated.

Fig. 11 shows the single crystal X-ray diffractogram of Pt_1/MOF, where the single Pt atoms are marked with an arrow.[38b] As can be seen, the MOF is constituted by ~1 nm channels with homogeneously distributed isolated Pt atoms stabilized on the framework walls by electronic interactions.[35,38b,d] This structure resembles that expected in the cavities and channels of the zeolite and, thus, it is not surprising that the Pt_1-supported microporous MOF catalyses the hydrosilylation of alkenes similarly or even better than Pt_1/NaY does. Fig. 11 also shows the scope for the hydrosilylation of terminal alkenes catalysed by Pt_1/MOF, and not only aromatic (products **18–23**) but also alkyl alkenes (products **24–25**) engage well in the reaction. Different electron poor silanes are reactive, including $PhSiH_3$ as a selective monosilylation partner; however, triethylsilane **2** was not suitable in this case.

A hot filtration test for the hydrosilylation of styrene **16** with the Pt_1/MOF catalyst shows that the ~30% of the catalytic activity comes from active species in solution (Fig. S27,† left); however, most of the catalytic activity lies in the solid under reaction conditions. Furthermore, when one looks at the kinetic profile closely, a short but clear induction time of 5 min can be seen (Fig. S28,† right), an induction time that is not present at all when the hydrosilylation of **16** is catalyzed even by tiny amounts of Karstedt's catalyst in solution, according to our experiments (Fig. S29†). The induction time with Pt_1/MOF may indicate that initial Pt_1 on the MOF is not the active species and evolves to active Pt_1 during the reaction. Coulombic forces are behind the stabilization of Pt on the negatively-charge walls of the microporous solids. Thus subtle electronic modifications of the Pt_1 atom by donation of electron density from the solid framework to the metal atom could modulate and ultimately increase the catalytic activity.[45] Indeed, by just heating Pt_1/NaY in an oven at 200 °C for 1 hour before the reaction, the hydrosilylation of **16** proceeds with full conversion and with the highest TOF measured (entry 9 in Table 2). X-ray photoelectron spectroscopy (XPS) in combination with CO-probe low temperature infrared (IR) measurements of the Pt_1/NaY sample calcined at 200 °C show that the amount of Pt(0) increases at least twice with respect to Pt(II) in non-calcined Pt_1/NaY and Pt_1/MOF (Fig. S29†). These results support the formation of catalytically active, reduced Pt_1 species within the microporous catalyst. It should be noted that the Pt_1 annotation used here does not necessarily presuppose hardly reduced species, since discussion focuses on Pt atomicity rather than on the exact valence state.

2.2.3 Dehydrogenative hydrosilylation of alcohols. Both the hydrosilylation of carbonyl compounds (aldehydes and ketones)[46] and the dehydrogenative hydrosilylation of alcohols[47] lead to the same *O*-silylated products (see Fig. 1), which are classical functional groups to protect alcohols, carry out additional manipulations in the molecule or finally recover the alcohol functionality after deprotection, or even trigger unexpected reactions.[48] Besides, alcohols are common precursors for

carbonyl compounds (by oxidation) and are widely available and stable compounds, particularly primary alcohols. In view of this, we studied here the direct hydrosilylation of alcohols and not carbonyl hydrosilylation, the former usually performed with other soluble catalysts rather than Pt[49] despite very early studies showing that Speier's catalyst $H_2PtCl_6 \cdot 6H_2O$ was catalytically active in solution,[50] and that simple metal nanoparticles can also catalyse the reaction.[47,51] First, the catalytic performance of Karstedt's catalyst at ppm for the hydrosilylation of 1-octanol **26** with dimethylphenylsilane **17** was studied, and the results (Table S13†) show that, after optimization of the reactants, solvent and catalyst amount, and reaction temperature and time, octyldimethylphenylsiloxane **27** can be produced in 96% yield with just 100 ppm of Pt in 1,4-dioxane as the solvent of choice. With this result in hand, different soluble and solid Pt catalysts were tested, and the results are shown in Table 3.

Karstedt's catalyst is the only efficient soluble Pt catalyst from those tested (entries 1–4), and considering that Karstedt's catalyst only contains Pt(0) atoms, and that Pt/C is also quite effective (entry 5), it seems that Pt(0) could be the active redox species for the dehydrogenative silylation of alcohols. This hypothesis fits well with the studies above on alkynes and alkenes and also with the lower activity shown by $PtCl_2/SiO_2$ and Pt_1/MOF (entries 6 and 7) with respect to Pt_1/NaY (entry 8), which is able to easily modulate the Pt site by the negatively-charged zeolite framework. Indeed, Pt_1/NaY calcined at 200 °C, which tends to reduce the Pt atoms further,[38a] gives a 99% yield of **27** and the highest initial TOF (entry 9). Calcination at higher temperatures to provoke metal aggregation (entry 10),[52] and decreasing or increasing the electronic density of the zeolite with a different charge compensating cation to Na^+ (H^+ and Cs^+, entries 11 and 12 respectively),[38a] do not improve the catalytic activity and supports the need of fine tuning the Pt site on truly heterogeneous microporous solid catalysts for the hydrosilylation reaction, when leaching does not occur (Fig. S30†). These facts point again to an *in situ* formation of the Pt catalyst, and having in mind the H-atom bridges found in the metal(oid) cluster intermediates and the decisive effect of the zeolite confined space, it is possible to propose a tentative mechanism for the dehydrogenative silylation of alcohols based on metal(oid) cycles (Fig. S31†).[53] Although speculative, this mechanism should be taking into consideration for future catalyst design based on Pt for the dehydrogenative hydrosilylation of alcohols.

Table 3 Results for the dehydrogenative hydrosilylation of 1-octanol **26** with dimethylphenylsilane **17** to give octyldimethylphenylsiloxane **27** with different Pt catalysts (100 ppm); acac = acetylacetonate, COD = cyclooctadiene. GC yields using *n*-dodecane as an external standard

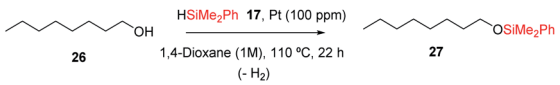

26 **27**

Entry	Pt catalyst	Yield (%)	TOF_0 (h^{-1})
1	Karstedt	96	126
2	$Pt(acac)_2$	26	30
3	$Pt(NH_3)_4Cl_2 \cdot xH_2O$	33	37
4	$Pt(COD)(Me)_2$	38	43
5	Pt/C	87	99
6	$PtCl_2/SiO_2$	37	42
7	Pt_1/MOF	35	42
8	Pt_1/NaY	93	106
9	**Pt_1/NaY (calc. at 200 °C)**	**99**	**118**
10	Pt_1/NaY (calc. at 300 °C)	64	76
11	Pt_1/HY	61	72
12	Pt_1/CsY	19	22
13	Pt_3/NaY	22	26

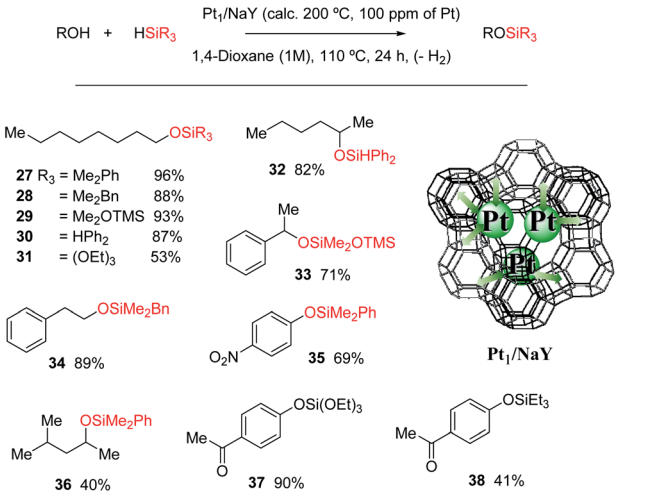

Fig. 12 Schematic representation of the Pt_1/NaY catalyst and catalytic activity for the dehydrogenative hydrosilylation of different alcohols with silanes under the indicated reaction conditions. GC yields using *n*-dodecane as an external standard. Products were generally not isolated.

Fig. 12 shows that the Pt_1/NaY solid calcined at 200 °C for 1 hour, catalyses the dehydrogenative hydrosilylation of alkyl alcohols (products **28–32**, **34** and **36**), benzyl alcohols (product **33**) and phenol derivatives (products **34** and **37–38**) in good yields and with just 100 ppm of Pt, and with different silanes. Interestingly, the disilane H_2SiPh_2 yields only the monosilylated product without further reaction, and the silane $HSi(OEt)_3$ was also reactive in this case, to give products **30** and **37**, respectively, in very good yields. To our knowledge, this is the first Pt-based efficient solid catalyst for the dehydrogenative hydrosilylation of alcohols.

3 Conclusions

The regioselectivity of the Pt-catalysed hydrosilylation of alkynes is controlled by *in situ* formed cyclic Pt–silane metal(-oid) clusters, and while the cluster formed by one Pt atom and two silane molecules leads to the β-(*E*)-vinylsilane product, the cluster formed by three Pt atoms and one silane molecule leads to the α-vinylsilane product. These cyclic unstrained transition states lower the activation energies of the reaction by facilitating the rate determining step of the reaction, *i.e.* the oxidative addition of the silane. These Pt intermediates are, in principle, suitable to be stabilized within the nanometric confined space

of zeolites and MOFs, and indeed, the Pt-supported solids catalyse very efficiently not only the hydrosilylation of alkynes but also of alkenes and the dehydrogenative hydrosilylation of alcohols, and can be recycled. These results provide a plausible alternative mechanism for the long-accepted Chalk–Harrod mechanism and give tools to design new hydrosilylation reactions based on ppm of Pt, of relevance in industrial chemistry.

Conflicts of interest

There are no conflicts of interest to declare.

Acknowledgements

Financial support by MINECO through the Severo Ochoa program (SEV-2016-0683), Excellence program (CTQ 2017-86735-P and CTQ 2017-87974-R) and Retos Col. (RTC-2017-6331-5) is acknowledged. E. P. acknowledges the financial support of the European Research Council under the European Union's Horizon 2020 research and innovation program/ERC Grant Agreement No. 814804, MOF-reactors. M. A. R.-C. thanks ITQ for the concession of a contract and J. O. M. thanks the Juan de la Cierva program for the concession of a contract. We thank V. B. dLL. and N. G. G. for performing degree projects in the ITQ labs. This research was partially supported by the supercomputing infrastructure of Poznan Supercomputing Center. The Electron Microscopy Service of the UPV is also acknowledged.

Notes and references

1 (*a*) B. M. Trost and Z. T. Ball, *Synthesis*, 2005, 853–887For a book see(*b*) B. Marciniec, H. Maciejewski, C. Pietrasuk and P. Pawluc, *Hydrosilylation: A Comprehensive review on Recent Advances*, Springer, Netherlands, 2009.

2 For some recent studies see(*a*) P.-W. Long, X.-F. Bai, F. Ye, L. Li, Z. Xu, K.-F. Yang, Y.-M. Cui, Z.-J. Zheng and L.-W. Xu, *Adv. Synth. Catal.*, 2018, **360**, 2825–2830; (*b*) A. A. Szymaniak, C. Zhang, J. R. Coombs and J. P. Morken, *ACS Catal.*, 2018, **8**, 2897–2901; (*c*) C. Dong, Y. Yuan, Y.-M. Cui, Z.-J. Zheng, J. Cao, Z. Xu and L.-W. Xu, *Appl. Organomet. Chem.*, 2018, **32**, e4037; (*d*) Y. Zhu, T. Cao, C. Cao, J. Luo, W. Chen, L. Zheng, J. Dong, J. Zhang, Y. Han, Z. Li, C. Chen, Q. Peng, D. Wang and Y. Li, *ACS Catal.*, 2018, **8**, 10004–10011; (*e*) M. A. Guseva, D. A. Alentiev, E. V. Bermesheva, I. A. Zamilatskovc and M. V. Bermeshev, *RSC Adv.*, 2019, **9**, 33029–33037; (*f*) L. Chen, I. S. Ali, G. E. Sterbinsky, J. T. L. Gamler, S. E. Skrabalak and S. L. Tait, *ChemCatChem*, 2019, **11**, 2843–2854; (*g*) J. Walkowiak, K. Salamon, A. Franczyk, K. Stefanowska, J. Szyling and I. Kownacki, *J. Org. Chem.*, 2019, **84**, 2358–2365.

3 For a recent review see:(*a*) J. V. Obligacion and P. J. Chirik, *Nat. Rev. Chem.*, 2018, **2**, 15–34For a representative example see(*b*) I. Pappas, S. Treacy and P. J. Chirik, *ACS Catal.*, 2016, **6**, 4105–4109.

4 A. Corma, C. González-Arellano, M. Iglesias and F. Sánchez, *Angew. Chem., Int. Ed.*, 2007, **46**, 7820–7822.

5 For a review see:(*a*) M. Pagliaro, R. Ciriminna, V. Pandarus and F. Béland, *Eur. J. Org. Chem.*, 2013, 6227–6235; (*b*) For a representative study see: X. Cui, K. Junge, X. Dai, C. Kreyenschulte, M.-M. Pohl, S. Wohlrab, F. Shi, A. Brückner and M. Beller, *ACS Cent. Sci.*, 2017, **3**, 580–585.

6 T. K. Meister, K. Riener, P. Gigler, J. Stohrer, W. A. Herrmann and F. E. Kühn, *ACS Catal.*, 2016, **6**, 1274–1284.

7 L. N. Lewis, K. G. Sy, G. L. Bryant and P. E. Donahue, *Organometallics*, 1991, **10**, 3750–3759.

8 (*a*) N. Asao, T. Sudo and Y. Yamamoto, *J. Org. Chem.*, 1996, **61**, 7654–7655; (*b*) L. Yong, K. Kirleis and H. Butenschön, *Adv. Synth. Catal.*, 2006, **348**, 833–836; (*c*) V. S. Sridevi, W. Y. Fan and W. K. Leong, *Organometallics*, 2007, **26**, 1157–1160.

9 M. A. Rivero-Crespo, A. Leyva-Perez and A. Corma, *Chem.–Eur. J.*, 2017, **23**, 1702–1708.

10 G. Longoni and P. Chini, *J. Am. Chem. Soc.*, 1976, **98**, 7225–7231.

11 J. C. Calabrese, L. F. Dahl, P. Chini, G. Longoni and S. Martinengo, *J. Am. Chem. Soc.*, 1974, **96**, 2614–2616.

12 (*a*) R. S. Tanke and R. H. Crabtree, *J. Chem. Soc., Chem. Commun.*, 1990, 1056–1057; (*b*) A. Sato, H. Kinoshita, H. Shinokubo and K. Oshima, *Org. Lett.*, 2004, **6**, 2217–2220; (*c*) G. de Bo, G. Berthon-Gelloz, B. Tinant and I. E. Markó, *Organometallics*, 2006, **25**, 1881–1890; (*d*) M. V. Jiménez, J. J. Pérez-Torrente, M. I. Bartolomé, V. Gierz, F. J. Lahoz and L. A. Oro, *Organometallics*, 2008, **27**, 224–234.

13 L. Ortega-Moreno, R. Peloso, C. Maya, A. Suárez and E. Carmona, *Chem. Commun.*, 2015, **51**, 17008–17011.

14 For induction times directly related to catalytically-active metal cluster formation, see for instance:(*a*) J. Oliver-Meseguer, J. R. Cabrero-Antonino, I. Dominguez, A. Leyva-Perez and A. Corma, *Science*, 2012, **338**, 1452–1455; (*b*) A. Leyva-Pérez, J. Oliver-Meseguer, P. Rubio-Marqués and A. Corma, *Angew. Chem., Int. Ed.*, 2013, **52**, 11554–11559; (*c*) J. Oliver-Meseguer, L. Liu, S. Garcia-Garcia, C. Canos-Gimenez, I. Dominguez, R. Gavara, A. Domenech-Carbo, P. Concepcion, A. Leyva-Perez and A. Corma, *J. Am. Chem. Soc.*, 2015, **137**, 3894–3900.

15 (*a*) M. A. Esteruelas, M. Oliván, L. A. Oro and J. Tolosa, *J. Organomet. Chem.*, 1995, **487**, 143–149; (*b*) R. Takeuchi, S. Nitta and D. Watanabe, *J. Org. Chem.*, 1995, **60**, 3045–3051.

16 B. G. M. Rocha, E. A. Valishina, R. S. Chay, M. F. C. Guedes da Silva, T. M. Buslaeva, A. J. L. Pombeiro, V. Y. Kukushkin and K. V. Luzyanin, *J. Catal.*, 2014, **309**, 79–86.

17 E. J. Rayment, N. Summerhill and E. A. Anderson, *J. Org. Chem.*, 2012, **77**, 7052–7060.

18 (*a*) V. P. Ananikov and I. P. Beletskaya, *Organometallics*, 2012, **31**, 1595–1604; (*b*) A. V. Astakhov, O. V. Khazipov, A. Y. Chernenko, D. V. Pasyukov, A. S. Kashin, E. G. Gordeev, V. N. Khrustalev, V. M. Chernyshev and V. P. Ananikov, *Organometallics*, 2017, **36**, 1981–1992.

19 (*a*) D. G. Blackmond, *Angew. Chem., Int. Ed.*, 2005, **44**, 4302–4320; (*b*) D. G. Blackmond, *Angew. Chem.*, 2005, **117**, 4374–

4393; (*c*) D. G. Blackmond, *J. Am. Chem. Soc.*, 2015, **137**, 10852–10866.

20 (*a*) J. Burés, *Angew. Chem., Int. Ed.*, 2016, **55**, 16084–16087; (*b*) J. Burés, *Angew. Chem., Int. Ed.*, 2016, **55**, 2028–2031.

21 (*a*) J. S. Mathew, M. Klussmann, H. Iwamura, F. Valera, A. Futran, E. A. C. Emanuelsson and D. G. Blackmond, *J. Org. Chem.*, 2006, **71**, 4711–4722; (*b*) M. Colladon, A. Scarso, P. Sgarbossa, R. A. Michelin and G. Strukul, *J. Am. Chem. Soc.*, 2007, **129**, 7680–7689; (*c*) R. D. Baxter, D. Sale, K. M. Engle, J.-Q. Yu and D. G. Blackmond, *J. Am. Chem. Soc.*, 2012, **134**, 4600–4606; (*d*) S. B. Kedia and M. B. Mitchell, *Org. Process Res. Dev.*, 2009, **13**, 420–428.

22 (*a*) E. V. Anslyn and D. A. Dougherty, *Modern Physical Organic Chemistry*, University Science Books, 2006; (*b*) A. K. Cook and M. S. Sanford, *J. Am. Chem. Soc.*, 2015, **137**, 3109–3118; (*c*) L. Legnani, G. Prina-Cerai, T. Delcaillau, S. Willems and B. Morandi, *Science*, 2018, **362**, 434–439; (*d*) K. C. Aroh and K. F. Jensen, *React. Chem. Eng.*, 2018, **3**, 94–101.

23 E. Fernandez, M. A. Rivero-Crespo, I. Dominguez, P. Rubio-Marques, J. Oliver-Meseguer, L. Liu, M. Cabrero-Antonino, R. Gavara, J. C. Hernandez-Garrido, M. Boronat, A. Leyva-Perez and A. Corma, *J. Am. Chem. Soc.*, 2019, **141**, 1928–1940.

24 S. Sakaki, N. Mizoe and M. Sugimoto, *Organometallics*, 1998, **17**, 2510–2523.

25 (*a*) M. Tanabe, D. Ito and K. Osakada, *Organometallics*, 2007, **26**, 459–462; (*b*) B. J. Anderson, J. A. Keith and M. S. Sigman, *J. Am. Chem. Soc.*, 2010, **132**, 11872–11874; (*c*) E. Tkatchouk, N. P. Mankad, D. Benitez, W. A. Goddard III and F. D. Toste, *J. Am. Chem. Soc.*, 2011, **133**, 14293–14300.

26 R. F. Weitkamp, B. Neumann, H.-G. Stammler and B. Hoge, *Angew. Chem., Int. Ed.*, 2020, **59**, 5494–5499.

27 H. Yang, K. T. Kotz, M. C. Asplund and C. B. Harris, *J. Am. Chem. Soc.*, 1997, **119**, 9564–9565.

28 (*a*) C. A. Tsipis, *J. Organomet. Chem.*, 1980, **187**, 427–446; (*b*) D. A. Rooke, Z. A. Menard and E. M. Ferreira, *Tetrahedron*, 2014, **70**, 4232–4244; (*c*) D. A. Rooke and E. M. Ferreira, *Angew. Chem., Int. Ed.*, 2012, **51**, 3225–3230.

29 A. Hamze, O. Provot, M. Alami and J.-D. Brion, *Org. Lett.*, 2005, **7**, 5625–5628.

30 M. Alami, F. Liron, M. Gervais, J.-F. Peyrat and J.-D. Brion, *Angew. Chem., Int. Ed.*, 2002, **41**, 1578–1580.

31 M. Rubin, A. Trofimov and V. Gevorgyan, *J. Am. Chem. Soc.*, 2005, **127**, 10243–10249.

32 (*a*) For a review see: J. Y. Corey, *Chem. Rev.*, 2011, **111**, 863–1071For representative references see:(*b*) L. M. Bavaro, P. Montangero and J. B. Keister, *J. Am. Chem. Soc.*, 1983, **105**, 4977–4981; (*c*) K. Osakada, M. Tanabe and T. Tanase, *Angew. Chem., Int. Ed.*, 2000, **39**, 4053–4055; (*d*) M. Itazaki, O. Kitami, M. Tanabe, Y. Nishihara and K. Osakada, *J. Organomet. Chem.*, 2005, **690**, 3957–3962.

33 J. M. Chance and T. A. Nile, *J. Mol. Catal.*, 1987, **42**, 91–97.

34 M. Mon, M. A. Rivero-Crespo, J. Ferrando-Soria, A. Vidal-Moya, M. Boronat, A. Leyva-Perez, A. Corma, J. C. Hernandez-Garrido, M. Lopez-Haro, J. J. Calvino, G. Ragazzon, A. Credi, D. Armentano and E. Pardo, *Angew. Chem., Int. Ed.*, 2018, **57**, 6186–6191.

35 F. R. Fortea-Perez, M. Mon, J. Ferrando-Soria, M. Boronat, A. Leyva-Perez, A. Corma, J. M. Herrera, D. Osadchii, J. Gascon, D. Armentano and E. Pardo, *Nat. Mater.*, 2017, **16**, 760–766.

36 A. Corma, R. Juárez, M. Boronat, F. Sánchez, M. Iglesias and H. García, *Chem. Commun.*, 2011, **47**, 1446–1448.

37 M. Boronat and A. Corma, *ACS Catal.*, 2019, **9**, 1539–1548.

38 (*a*) P. Rubio-Marques, M. A. Rivero-Crespo, A. Leyva-Perez and A. Corma, *J. Am. Chem. Soc.*, 2015, **137**, 11832–11837; (*b*) M. A. Rivero-Crespo, M. Mon, J. Ferrando-Soria, C. W. Lopes, M. Boronat, A. Leyva-Perez, A. Corma, J. C. Hernandez-Garrido, M. Lopez-Haro, J. J. Calvino, E. V. Ramos-Fernandez, D. Armentano and E. Pardo, *Angew. Chem., Int. Ed.*, 2018, **57**, 17094–17099; (*c*) K. Kratzl, T. Kratky, S. Günther, O. Tomanec, R. Zbořil, J. Michalička, J. M. Macak, Mi. Cokoja and R. A. Fischer, *J. Am. Chem. Soc.*, 2019, **141**, 13962–13969; (*d*) N. Van Velthoven, S. Waitschat, S. M. Chavan, P. Liu, S. Smolders, J. Vercammen, B. Bueken, S. Bals, K. P. Lillerud, N. Stock and D. E. De Vos, *Chem. Sci.*, 2019, **10**, 3616–3622.

39 A. I. Serykh, O. P. Tkachenko, V. Y. Borovkov, V. B. Kazansky, M. Beneke, N. I. Jaeger and G. Schulz-Ekloff, *Phys. Chem. Chem. Phys.*, 2000, **2**, 5647–5652.

40 J. de Graaf, A. J. van Dillen, K. P. de Jong and D. C. Koningsberger, *J. Catal.*, 2001, **203**, 307–321.

41 β-(*E*)-Vinylsilanes are the typical products, see for instance: Y. Ishikawa, Y. Yamamoto and N. Asao, *Catal. Sci. Technol.*, 2013, **3**, 2902–2905.

42 (*a*) B. Kopping, C. Chatgilialoglu, M. Zehnder and B. Giese, *J. Org. Chem.*, 1992, **57**, 3994–4000; (*b*) K. Liu, X. Shen, S. Bai and Z. C. Zhang, *ChemCatChem*, 2020, **12**, 267–272.

43 Y. Chen, S. Ji, W. Sun, W. Chen, J. Dong, J. Wen, J. Zhang, Z. Li, L. Zheng, C. Chen, Q. Peng, D. Wang and Y. Li, *J. Am. Chem. Soc.*, 2018, **140**, 7407–7410.

44 T. Galeandro-Diamant, M.-L. Zanota, R. Sayah, L. Veyre, C. Nikitine, C. de Bellefon, S. Marrot, V. Meille and C. Thieuleux, *Chem. Commun.*, 2015, **51**, 16194–16196.

45 (*a*) Y. Zhu, T. Cao, C. Cao, J. Luo, W. Chen, L. Zheng, J. Dong, J. Zhang, Y. Han, Z. Li, C. Chen, Q. Peng, D. Wang and Y. Li, *ACS Catal.*, 2018, **8**, 10004–10011; (*b*) C. J. Kong, S. E. Gilliland, B. R. Clark and B. F. Gupton, *Chem. Commun.*, 2018, **54**, 13343–13346; (*c*) L. Chen, I. S. Ali, G. E. Sterbinsky, J. T. L. Gamler, S. E. Skrabalak and S. L. Tait, *ChemCatChem*, 2019, **11**, 2843–2854; (*d*) B. B. Sarma, J. Kim, J. Amsler, G. Agostini, C. Weidenthaler, N. Pfänder, R. Arenal, P. Concepción, P. Plessow, F. Studt and G. Prieto, *Angew. Chem., Int. Ed.*, 2020, **59**, 5806–5815.

46 Z. Zuo, H. Sun, L. Wang and X. Li, *Dalton Trans.*, 2014, **43**, 11716–11722.

47 J. F. Blandez, A. Primo, A. M. Asiri, M. Álvaro and H. García, *Angew. Chem., Int. Ed.*, 2014, **53**, 12581–12586.

48 L. L. Adduci, T. A. Bender, J. A. Dabrowski and M. R. Gagné, *Nat. Chem.*, 2015, **7**, 576–581.

49 (*a*) A. A. Toutov, K. N. Betz, M. C. Haibach, A. M. Romine and R. H. Grubbs, *Org. Lett.*, 2016, **18**, 5776–5779; (*b*) V. Ritleng, M. Henrion and M. J. Chetcuti, *ACS Catal.*, 2016, **6**, 890–906;

(*c*) X. Dong, A. Weickgenannt and M. Oestreich, *Nat. Commun.*, 2017, **8**, 15547; (*d*) D. Ventura-Espinosa, A. Carretero-Cerdán, M. Baya, H. García and J. A. Mata, *Chem.–Eur. J.*, 2017, **23**, 10815–10821.

50 L. H. Sommer and J. E. Lyons, *J. Am. Chem. Soc.*, 1969, **91**, 7061–7067.

51 S. Pramanik, A. Fernandes, V. Liautard, M. Pucheault, F. Robert and Y. Landais, *Chem.–Eur. J.*, 2019, **25**, 728–732.

52 (*a*) W. Gao, P. Tieu, C. Addiego, Y. Ma, J. Wu and X. Pan, *Sci. Adv.*, 2019, **5**, eaau9590; (*b*) B. H. Kim, J. Heo, S. Kim, C. F. Reboul, H. Chun, D. Kang, H. Bae, H. Hyun, J. Lim, H. Lee, B. Han, T. Hyeon, A. P. Alivisatos, P. Ercius, H. Elmlund and J. Park, *Science*, 2020, **368**, 60–67.

53 E. M. Simmons and J. F. Hartwig, *J. Am. Chem. Soc.*, 2010, **132**, 17092–17095.